

Solar Forecasting with Causality: A Graph-Transformer Approach to Spatiotemporal Dependencies

Yanan Niu*

EPFL

Lausanne, Switzerland

yanan.niu@epfl.ch

Christophe Moser

EPFL

Lausanne, Switzerland

christophe.moser@epfl.ch

Demetri Psaltis

EPFL

Lausanne, Switzerland

demetri.psaltis@epfl.ch

Luisa Lambertini†

EPFL

Lausanne, Switzerland

luisa.lambertini@epfl.ch

Abstract

Accurate solar forecasting underpins effective renewable energy management. We present **SolarCAST**, a causally informed model predicting future global horizontal irradiance (GHI) at a target site using only historical GHI from site X and nearby stations S —unlike prior work that relies on sky-camera or satellite imagery requiring specialized hardware and heavy preprocessing. To deliver high accuracy with only public sensor data, SolarCAST models three classes of confounding factors behind $X-S$ correlations using scalable neural components: (i) observable synchronous variables (e.g., time of day, station identity), handled via an embedding module; (ii) latent synchronous factors (e.g., regional weather patterns), captured by a spatio-temporal graph neural network; and (iii) time-lagged influences (e.g., cloud movement across stations), modeled with a gated transformer that learns temporal shifts. It outperforms leading time-series and multimodal baselines across diverse geographical conditions, and achieves a 25.9% error reduction over the top commercial forecaster, *Solcast*. **SolarCAST** offers a lightweight, practical, and generalizable solution for localized solar forecasting.¹

CCS Concepts

- Computing methodologies → Neural networks.

Keywords

Solar Forecasting; Spatiotemporal Data; Causal Inference; Graph Neural Networks; Transformer

ACM Reference Format. Yanan Niu, Demetri Psaltis, Christophe Moser, and Luisa Lambertini. 2025. Solar Forecasting with Causality: A Graph-Transformer Approach to Spatiotemporal Dependencies. In *Proceedings of the 34th ACM International Conference on Information and Knowledge Management (CIKM '25), November 10–14, 2025, Seoul, Republic of Korea*. ACM, New York, NY, USA, 5 pages. <https://doi.org/10.1145/3746252.3760905>

*Corresponding author

†Also with Università della Svizzera italiana (USI).

¹Code available at <https://github.com/YananNiu/SolarCAST>

1 Introduction

By the end of 2024, global solar photovoltaic capacity surpassed 2.2 terawatts, providing over 10% of the world’s electricity and accounting for more than 75% of new renewable generation [1]. As solar power becomes a cornerstone of modern energy systems, precise short-term forecasting of solar irradiance is critical for grid stability, energy storage optimization, and energy market operations.

Traditional solar forecasting models typically rely on historical global horizontal irradiance (GHI) measurements at a single target site. However, these point-based models often struggle under dynamic weather conditions—particularly when clouds move rapidly across the sky. To address this, researchers have explored auxiliary inputs such as all-sky images [4], panoramic cameras [12], or satellite imagery [16]. While these sources can enhance short-term predictions by providing broader spatial context, many depend on specialized hardware or remote sensing access. Also, they offer only indirect visual cues about local irradiance, making them less reliable under poor image quality or limited coverage.

In this work, we explore a less-tapped yet increasingly abundant auxiliary input for localized solar forecasting: GHI measurements from nearby weather stations. These data are now widely available across many countries², offering structured numerical signals with explicit physical meaning. Compared to imagery-based proxies, these time-series inputs are easier to preprocess and integrate, avoiding the need for complex image processing pipelines. Combining the target location’s GHI sequence X with auxiliary sequences S from nearby stations yields a spatio-temporal (ST) multivariate time series (MTS). A forecasting model is then applied to predict future GHI values at the target site, framing the task as an MTS prediction problem with a single target output.

To better leverage ST solar data, we adopt a causal perspective: while S serves as auxiliary input for forecasting future GHI at the target site X , both may be influenced by shared confounders. We identify three key types: (1) Observable synchronous confounders (e.g., time of day, node identity) that affect all sensors simultaneously; (2) Latent synchronous confounders, such as regional weather patterns that create shared but unobserved influences across locations; and (3) Time-lagged causal drivers, like moving clouds, which introduce delayed, directional dependencies across space and time.

²For example, Switzerland’s MeteoSwiss <https://www.meteoswiss.admin.ch/> and the U.S. National Solar Radiation Database <https://nsrdb.nrel.gov>.

These causal patterns call for models that capture both synchronous and asynchronous ST interactions. For synchronous effects, spatio-temporal graph neural networks (STGNNs) offer a natural fit, and have demonstrated strong performance in domains like traffic forecasting [7, 11, 23, 25], neuroscience [10], and recommendation systems [22]. By representing sensor relationships as a graph, STGNNs allow each node to aggregate information from spatial neighbors at the same time step, effectively modeling shared environmental influences. However, most existing STGNNs treat space and time separately, typically applying recurrent neural networks (RNNs), convolutional neural networks (CNNs), or other temporal modules before or after graph-based message passing [2, 5]. This “time-then-graph” structure models spatial and temporal dependencies separately. However, this separation limits its ability to capture asynchronous, non-local interactions—such as a moving cloud affecting one sensor at time t and another at $t + \Delta$. Since these patterns require joint modeling of spatiotemporal causality, we propose **SolarCAST**, a Causal-Aware Spatio-Temporal predictor, designed to more effectively capture both synchronous and asynchronous cross-series dependencies:

- An **embedding layer** encodes observable synchronous confounders for X and S , such as time and station identity.
- A **STGNN module** implicitly captures synchronous *long-term, stable spatial dependencies* between X and S .
- A **Gated Transformer module** explicitly models *non-regular, non-local ST interactions*. Its self-attention mechanism captures arbitrary dependencies across time and space, enabling the model to track causal patterns with temporal shifts. A gating mechanism filters out spurious correlations, emphasizing high-impact, informative relationships.

SolarCAST is lightweight and scalable, making it well-suited for real-world deployment across diverse geographic regions, even with sparse or uneven sensor distributions. It outperforms strong MTS baselines and multimodal models using image-based inputs, demonstrating the effectiveness of nearby GHI as a practical data source for this task. Compared to a commercial solar forecasting provider, Solcast³, **SolarCAST** achieves a 25.9% improvement in localized solar forecasting accuracy, highlighting its practical value.

2 Framework

Let $X = \{x_{t-T:t}\} \in \mathbb{R}^{T \times d}$ denote the historical features at the target node, i.e., GHI at the forecasting site over a window of T time steps. Similarly, let $S = \{s_{t-T:t}^i\}_{i=1}^{N-1} \in \mathbb{R}^{T \times d}$ represent the historical features from $N - 1$ auxiliary nodes, corresponding to nearby GHI sensors, which may be spatially sparse or unevenly distributed. The objective is to predict the GHI at the target node at a future time step, $x_{t+h} := y$, given a prediction horizon h .

Previous MTS forecasting studies have adopted the Structural Causal Model (SCM) paradigm [13] to improve model interpretability through a causal view—for example, by applying causal treatments [20] or explicitly modeling confounders [8]. Following this direction, we also frame our problem using SCM to guide the architectural design of our model and enhance forecasting accuracy. Specifically, we identify three types of confounders that may underlie the observed correlations between X and S , see Fig. 1:

³<https://solcast.com/>

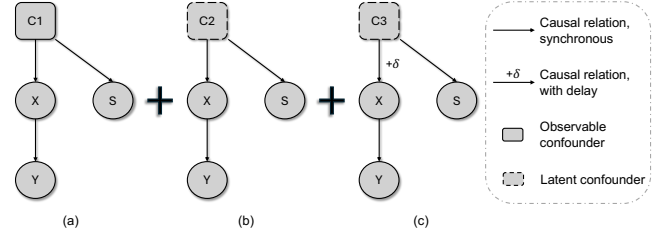


Figure 1: Illustration of the causal relationships underlying the correlation between the target and auxiliary sensors.

- **C1: Observable synchronous confounders**—such as time of day, season, or node identity—simultaneously influence both X and S .
- **C2: Latent synchronized confounders**—such as regional cloud cover or large-scale atmospheric phenomena—affect all nodes simultaneously, but are not directly observed.
- **C3: Temporal-lagged latent confounders**—such as moving clouds—impact the auxiliary nodes S first and then reach the target node X after a delay δ .

3 Model Design

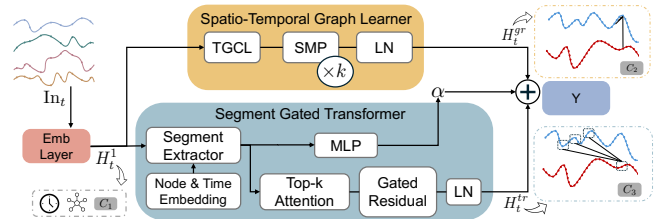


Figure 2: The pipeline of SolarCAST.

SolarCAST (Fig. 2) explicitly models each causal path identified in Fig. 1, aligning its architecture with the physical constraints and statistical dependencies in ST solar data. As input, the model takes a sequence of n historical time series, $\text{In}_t := (X_{t-T:t}, S_{t-T:t}^1, \dots, S_{t-T:t}^{(n-1)})$. To account for observable synchronous confounders (C_1), an *Embedding Layer* (EMB) augments each node’s feature representation with relevant contextual information. The resulting encoded features are then processed by two parallel modules: (1) a *Spatio-Temporal Graph Learner* (STGL) to capture spatially synchronized patterns (C_2), and (2) a *Segment Gated Transformer* (SGT) to model dynamic, lagged influences (C_3). The final output is computed as a learnable combination of the two pathways, weighted by a parameter α :

$$H_t^{(1)} = \text{EMB}(\text{In}_t) \quad (1a)$$

$$H_t^{gr} = \text{STGL}\left(H_t^{(1)}\right) \quad (1b)$$

$$H_t^{tr} = \text{SGT}\left(H_t^{(1)}\right), \quad \text{for } k = 3, \dots, K \quad (1c)$$

$$H_t^{out} = \alpha * H_t^{tr} + (1 - \alpha) * H_t^{gr} \quad (1d)$$

3.1 Embedding Layer

To control for observable synchronous confounders for $\text{In}_t \in \mathbb{R}^{n \times T \times d}$, we incorporate a *time-of-day embedding* $E_{\text{time}} \in \mathbb{R}^{T \times d_1}$ (capturing

temporal context based on sampling frequency) and a *node identity embedding* $E_{\text{node}} \in \mathbb{R}^{n \times d_2}$ (via a learnable lookup table which assigns a unique vector to each node). These auxiliary embeddings are concatenated with the input features along the dimension axis:

$$H_t^{(1)} = \text{Concat}(\text{In}_t, E_{\text{time}}, E_{\text{node}}) \in \mathbb{R}^{n \times T \times (d+d_1+d_2)}. \quad (2)$$

3.2 Spatio-Temporal Graph Learner

To capture synchronous but unobserved confounders (C_2) across sensor locations, we employ an STGL that propagates information via spatial message passing. A dynamic ST graph, $\mathcal{G}^t = (V, E, X_{t-T:t}, S_{t-T:t})$, is defined, where V is a set of n sensor nodes and E denotes the edges between them. The adjacency matrix $A \in \mathbb{R}^{n,n} : \{(i, j) : (i, j) \in E\}$ encodes node connectivity.

Unlike fixed-topology domains (e.g., traffic, power grids), solar networks lack structural connectivity since spatial proximity doesn't guarantee predictive relevance due to local cloud dynamics. We adopt a continuous, data-driven adjacency formulation inspired by Wu et al. [19] to learn soft, unidirectional dependencies, and avoid underfitting from static distance-based adjacency matrices or overfitting from fully end-to-end ones learned on small graphs:

$$M_1 = \tanh(E_1 W_1) \quad (3)$$

$$M_2 = \tanh(E_2 W_2) \quad (4)$$

$$\mathcal{A} = \sigma(M_1 M_2^T - M_2 M_1^T) \quad (5)$$

where all $E_{\{\cdot\}}$ are node embedding look-up tables, and all $W_{\{\cdot\}}$ are trainable weight matrices. The sigmoid activation $\sigma()$ produces dense, data-driven connectivity while avoiding excessive sparsity.

An STGL consists of a Temporal Gated Convolutional Layer (TGCL) for local temporal encoding, a Spatial Message Passing (SMP) module repeated K times (with $k = 3, \dots, K+2$) to handle both inflow and outflow information through each node, and a Layer Normalization (LN) layer for stability:

$$H_t^{(2)} = \text{TGCL}\left(H_t^{(1)}\right) \quad (6a)$$

$$H_t^{(k)} = \text{SMP}\left(H_t^{(2)}, H_t^{(k-1)}, \mathcal{A}\right) + \text{SMP}\left(H_t^{(2)}, H_t^{(k-1)}, \mathcal{A}^T\right) \quad (6b)$$

$$H_t^{gr} = \text{LN}(H_t^{(K+2)}) \quad (6c)$$

Temporal Gated Convolutional Layer. TGCL has been shown to improve performance in sequence modeling tasks [17–19]:

$$H_t^{(2)} = \tanh(H_t^{(1)} * W^f) \odot \sigma(H_t^{(1)} * W^g) \quad (7)$$

where $*$ denotes the convolution operator with kernel size k , and \odot indicates element-wise multiplication:

Spatial Message Passing. SMP adopts a graph convolutional network that performs multi-hop propagation over K steps [19]:

$$H_t^{(k)} = \beta H_t^{(2)} + (1 - \beta) \tilde{A} H_t^{(k-1)}, \quad \text{for } k = 3, \dots, K+2 \quad (8)$$

$$H_t^{gr} = \sum_{i=2}^{K+2} H_t^{(i)} W^{(i)} \quad (9)$$

where $\tilde{\mathcal{A}} = \tilde{D}^{-1}(\mathcal{A} + I)$, $\tilde{D}_{ii} = 1 + \sum_j \mathcal{A}_{ij}$, and β is a residual weight. The final output aggregates features from all propagation layers via an MLP for adaptive feature selection.

3.3 Segment Gated Transformer

We employ a transformer-based architecture augmented with cross-series attention to capture time-lagged and non-local dependencies across multiple time series. This mechanism allows the model to associate temporally distant segments and inter-series interactions, making it particularly effective for modeling dynamic propagation patterns, see Fig. 2. To improve robustness, we integrate a gating mechanism that selectively suppresses weak or noisy attention connections, highlighting the most informative ST dependencies.

Segment Extractor and Embeddings. Given input $H^{(1)} \in \mathbb{R}^{n \times T \times d'}$, we extract a query patch from the target node over the most recent q time steps, $H_{x,t-q:t}^{\text{query}} \in \mathbb{R}^{1 \times (q \cdot d')}$. Additionally, we collect m support patches of length l from all nodes, defined as $H_{t-r-p-l:t-r-p}^{\text{support}} \in \mathbb{R}^{(m \cdot n) \times (l \cdot d')}$ for $p = 0, \dots, m-1$. A fixed temporal gap r is enforced between the query and support segments to encourage the model to learn delayed dependencies between current and past information. Each segment is then projected into a representation of shape $\mathbb{R}^{1 \times d_{\text{model}}}$ via a linear layer. Temporal and structural context is incorporated for each patch using time embeddings and learnable node embeddings, similar to subsection 3.1.

Top-k Attention & Gated Residual. Tokens are passed through a transformer block with two key modifications. First, we apply a Top-K sparse multi-head attention mechanism in which each query attends only to its top-K most relevant support tokens per head. This design focuses attention on the most salient historical patterns, especially those reflecting delayed confounding effects (C_3). Second, we apply a Gated Linear Unit [3, 6] to the attention output before the residual connection. This gating re-weights feature channels, suppressing irrelevant signals and enhancing informative ones, thereby improving robustness without introducing extra sparsity.

Learnable α . A learnable scalar $\alpha \in (0, 1)$ dynamically weights the relative contribution of SGT and STGL on a per-sample basis,

$$\alpha = \sigma(W_1 \cdot \text{ReLU}(W_0 H^{\text{query}})) \quad (10)$$

It is computed from the query patch representation of the target node using an MLP, allowing the model to infer the relevance of time-lagged factors based on the current node state.

Table 1: Dataset summary.

Target	Range	# S	Dis.(km)	Camera des.
Urban(OO)	2021.12.7- 2024.12.31	7	7.8-37.4	360°, clear
Urban(SS)	2023.07.05- 2025.5.15	9	19.9-47.2	360°, noisy and small sky portion
Valley	2022.07.28- 2025.5.15	8	3.6-33.3	200°, foggy and small sky portion
Lake	2023.04.10- 2025.5.15	11	7.4-58.2	350°, strong wa- ter reflection
Mountain	2022.05.14- 2025.5.15	10	7.4-42.0	320°, foggy, snowy

Table 2: Comparison with benchmark methods across five datasets from diverse geographic regions. Lower RMSE and RSE, and higher CORR indicate better performance. The best results are shown in bold, and the second-best are underlined.

Model	Input	Urban (open space)			Urban (streetscape)			Valley			Lake			Mountain		
		RMSE	RSE	CORR	RMSE	RSE	CORR	RMSE	RSE	CORR	RMSE	RSE	CORR	RMSE	RSE	CORR
Persistent model [14]	X	100.039	0.694	0.758	161.390	0.541	0.855	179.402	0.585	0.818	140.514	0.490	0.879	152.097	0.536	0.858
SMT [12]	X, Img	74.228	0.515	0.858	152.368	0.511	0.865	123.201	0.402	0.917	130.209	0.454	0.894	142.725	0.503	0.866
LSTNet [9]	X, S	88.008	0.611	0.805	142.497	0.478	0.881	129.945	0.424	0.908	131.237	0.457	0.890	140.820	0.496	0.869
STID [15]	X, S	76.409	0.530	0.849	123.126	0.413	0.912	125.114	0.408	0.916	121.359	0.423	0.907	130.510	0.460	0.890
MTGNN [19]	X, S	<u>73.664</u>	<u>0.511</u>	<u>0.860</u>	127.283	0.427	0.905	121.660	0.397	0.920	120.534	0.420	0.908	126.186	0.444	0.897
TimeGNN [21]	X, S	78.492	0.545	0.842	123.350	<u>0.413</u>	<u>0.912</u>	120.741	0.394	0.919	120.192	0.419	0.913	<u>125.766</u>	0.443	<u>0.897</u>
SolarCAST	X, S	70.787	0.491	0.871	127.030	0.426	0.906	120.512	0.393	0.920	118.693	0.412	0.912	124.957	0.440	0.899

4 Experiments

4.1 Experimental Setup

Baselines. We compare against both solar forecasting and MTS models. For solar, we use the persistence model [14], a simple physical baseline, and SMT [12], a multimodal solar predictor. For MTS, we include LSTNet [9], a hybrid deep learning model; STID [24], a linear ST method; MTGNN [19], an STGNN benchmark; and TimeGNN [21], an STGNN that constructs graphs from timestamps to capture temporal dependencies. We also include a commercial forecasting solution from Solcast⁴ for practical benchmarking.

Data. We collect ST GHI data from weather stations operated by MeteoSwiss⁵. For each target location, nearby GHI measurements from surrounding stations serve as auxiliary time series. All data are sampled at 10-minute intervals. Tab. 1 summarizes the datasets, including landform type, data range, number and distance of auxiliary sensors to the target, and camera metadata (field of view and viewing conditions) used by SMT [12].

Implementation. SolarCAST is implemented in PyTorch 2.6.0 with time and node embeddings of dimension 10. The SGT module employs TGCL with kernel size 3 and SMP with depth $k = 3$. SGT pathway parameters include query/support patch lengths $l = 6$, $m = 9$, gap $r = 3, 4$ transformer heads and Top-5 attention. We use a 70/20/10 train/validation/test split with 2-hour prediction horizon at 10-minute resolution. Training employs MSE loss with AdamW optimizer (learning rate $1E - 3 \rightarrow 3E - 4$, polynomial decay factor 0.5, 20 epochs), and early stopping after 20 epochs of validation stagnation. Evaluation metrics include root mean square error (RMSE), root relative squared error (RSE), and correlation (CORR) [12].

4.2 Main Results

Comparisons with baseline models are presented in Tab. 2. To ensure a fair evaluation against the multimodal model SMT, which incorporates both X and Img [12], we restrict all testing to daylight hours when image data is available.⁶ As shown in Tab. 1, the quality and forecasting relevance of image data vary substantially across datasets due to differences in local climate and camera setup. SMT performs best with high-quality, clear panoramic images, as seen in the "Urban (Open Space)" dataset, where its results are comparable to or better than models using X and S . However, under less

favorable conditions, the contribution of image data declines. In contrast, auxiliary GHI data (S) consistently serves as an effective substitute for local visual input, even with sparse or uneven sensor deployment. This enables accurate localized forecasting without the need for dense image coverage, demonstrating the practicality of using S alongside X in our framework.

Models with ST identification, including STID [15], MTGNN [19], and TimeGNN [21], also perform strongly, leveraging topological priors through learned embeddings or explicit graphs to capture spatial correlations and suppress low-informative nodes. These methods align well with the nature of ST solar data.

SolarCAST builds on these strengths but is further tailored to ST solar forecasting by capturing time-lagged confounders that reflect delayed and dynamic weather effects. It achieves the best performance on 4 out of 5 datasets, demonstrating robustness across diverse geographic regions and sensor configurations. On a representative 12-day test set from March 2024, SolarCAST achieves an RMSE of 82.507, outperforming Solcast with an RMSE of 103.913, marking a 25.9% improvement. This result underscores the practical value of SolarCAST for accurate, real-world solar forecasting.

4.3 Ablations

Ablations on "Urban (Open Space)" dataset, shown in Tab. 3, validate the effectiveness of SolarCAST's three modules in addressing the corresponding types of confounders.

Table 3: Ablation study.

Metrics	SolarCAST	w/o EMB	w/o STGL	w/o SGT
RMSE	70.787	72.799	80.037	75.051
RSE	0.491	0.505	0.555	0.521
CORR	0.871	0.863	0.839	0.856

5 Conclusion

In this paper, we introduce SolarCAST, a causally informed spatiotemporal model that addresses confounders in solar forecasting using only publicly available time-series data. Its superior performance, combined with strong model interpretability, demonstrates high accuracy and strong real-world applicability.

Acknowledgments

This work was supported by the EPFL Solutions for Sustainability Initiative (S4S) grant. The authors thank Solcast for providing access to the data used in this study.

⁴<https://solcast.com/>

⁵<https://www.meteosuisse.admin.ch>

⁶Consequently, our error metrics are not directly comparable to those from public datasets that include nighttime periods, where near-zero irradiance values can artificially deflate errors.

References

[1] IEA PVPS TASK 1. 2025. *Global Market Outlook for Solar Power 2025–2029*. Technical Report. The International Energy Agency.

[2] Andrea Cini, Ivan Marisca, Daniele Zambon, and Cesare Alippi. 2023. Taming local effects in graph-based spatiotemporal forecasting. *Advances in Neural Information Processing Systems* 36 (2023), 55375–55393.

[3] Yann N Dauphin, Angela Fan, Michael Auli, and David Grangier. 2017. Language modeling with gated convolutional networks. In *International conference on machine learning*. PMLR, 933–941.

[4] Huiyu Gao and Miaoqiao Liu. 2022. Short-term Solar Irradiance Prediction from Sky Images with a Clear Sky Model. In *2022 IEEE/CVF Winter Conference on Applications of Computer Vision (WACV)*. 3074–3082. doi:10.1109/WACV51458.2022.00313

[5] Jianfei Gao and Bruno Ribeiro. 2022. On the equivalence between temporal and static equivariant graph representations. In *International Conference on Machine Learning*. PMLR, 7052–7076.

[6] Jonas Gehring, Michael Auli, David Grangier, Denis Yarats, and Yann N Dauphin. 2017. Convolutional sequence to sequence learning. In *International conference on machine learning*. PMLR, 1243–1252.

[7] Shengnan Guo, Youfang Lin, Huaiyu Wan, Xiucheng Li, and Gao Cong. 2021. Learning dynamics and heterogeneity of spatial-temporal graph data for traffic forecasting. *IEEE Transactions on Knowledge and Data Engineering* 34, 11 (2021), 5415–5428.

[8] Jiahao Ji, Wentao Zhang, Jingyuan Wang, and Chao Huang. 2025. Seeing the Unseen: Learning Basis Confounder Representations for Robust Traffic Prediction. In *Proceedings of the 31st ACM SIGKDD Conference on Knowledge Discovery and Data Mining (KDD '25)*. Association for Computing Machinery, New York, NY, USA. doi:10.1145/3690624.3709201

[9] Guokun Lai, Wei-Cheng Chang, Yiming Yang, and Hanxiao Liu. 2018. Modeling Long- and Short-Term Temporal Patterns with Deep Neural Networks. In *The 41st International ACM SIGIR Conference on Research & Development in Information Retrieval* (Ann Arbor, MI, USA) (SIGIR '18). Association for Computing Machinery, New York, NY, USA, 95–104. doi:10.1145/3209978.3210006

[10] Xiaoxiao Li, Yuan Zhou, Nicha Dvornek, Muhan Zhang, Siyuan Gao, Juntang Zhuang, Dustin Scheinost, Lawrence H Staib, Pamela Ventola, and James S Duncan. 2021. Braingnn: Interpretable brain graph neural network for fmri analysis. *Medical Image Analysis* 74 (2021), 102233.

[11] Yaguang Li, Rose Yu, Cyrus Shahabi, and Yan Liu. 2018. Diffusion Convolutional Recurrent Neural Network: Data-Driven Traffic Forecasting. In *International Conference on Learning Representations (ICLR '18)*.

[12] Yanan Niu, Roy Sarkis, Demetri Psaltis, Mario Paolone, Christophe Moser, and Luisa Lamberti. 2025. Solar Multimodal Transformer: Intraday Solar Irradiance Predictor Using Public Cameras and Time Series. In *2025 IEEE/CVF Winter Conference on Applications of Computer Vision (WACV)*. 5051–5060. doi:10.1109/WACV61041.2025.00494

[13] Judea Pearl. 2009. *Causality: Models, Reasoning and Inference* (2nd ed.). Cambridge University Press, USA.

[14] Hugo TC Pedro and Carlos FM Coimbra. 2012. Assessment of forecasting techniques for solar power production with no exogenous inputs. *Solar Energy* 86, 7 (2012), 2017–2028.

[15] Zezhi Shao, Zhao Zhang, Fei Wang, Wei Wei, and Yongjun Xu. 2022. Spatial-temporal identity: A simple yet effective baseline for multivariate time series forecasting. In *Proceedings of the 31st ACM international conference on information & knowledge management*. 4454–4458.

[16] Zhiyuan Si, Ming Yang, Yixiao Yu, and Tingting Ding. 2021. Photovoltaic power forecast based on satellite images considering effects of solar position. *Applied Energy* 302 (2021), 117514.

[17] Aaron van den Oord, Sander Dieleman, Heiga Zen, Karen Simonyan, Oriol Vinyals, Alex Graves, Nal Kalchbrenner, Andrew Senior, and Koray Kavukcuoglu. 2016. WaveNet: A Generative Model for Raw Audio. arXiv:1609.03499 [cs.SD] <https://arxiv.org/abs/1609.03499>

[18] Aaron van den Oord, Nal Kalchbrenner, Lasse Espeholt, koray kavukcuoglu, Oriol Vinyals, and Alex Graves. 2016. Conditional Image Generation with PixelCNN Decoders. In *Advances in Neural Information Processing Systems*, D. Lee, M. Sugiyama, U. Luxburg, I. Guyon, and R. Garnett (Eds.), Vol. 29. Curran Associates, Inc. https://proceedings.neurips.cc/paper_files/paper/2016/file/b130141feffabac455e1f90a7de2054-Paper.pdf

[19] Zonghan Wu, Shirui Pan, Guodong Long, Jing Jiang, Xiaojun Chang, and Chengqi Zhang. 2020. Connecting the Dots: Multivariate Time Series Forecasting with Graph Neural Networks. arXiv:2005.11650 [cs.LG] <https://arxiv.org/abs/2005.11650>

[20] Yutong Xia, Yuxuan Liang, Haomin Wen, Xu Liu, Kun Wang, Zhengyang Zhou, and Roger Zimmermann. 2023. Deciphering spatio-temporal graph forecasting: A causal lens and treatment. *Advances in Neural Information Processing Systems* 36 (2023), 37068–37088.

[21] Nancy Xu, Chrysoula Kosma, and Michalis Vaziriannis. 2023. TimeGNN: Temporal Dynamic Graph Learning for Time Series Forecasting. In *International Conference on Complex Networks and Their Applications*. Springer, 87–99.

[22] Rex Ying, Ruining He, Kaifeng Chen, Pong Eksombatchai, William L Hamilton, and Jure Leskovec. 2018. Graph convolutional neural networks for web-scale recommender systems. In *Proceedings of the 24th ACM SIGKDD international conference on knowledge discovery & data mining*. 974–983.

[23] Bing Yu, Haoteng Yin, and Zhanxing Zhu. 2018. Spatio-Temporal Graph Convolutional Networks: A Deep Learning Framework for Traffic Forecasting. In *Proceedings of the Twenty-Seventh International Joint Conference on Artificial Intelligence*. International Joint Conferences on Artificial Intelligence Organization, 3634–3640. doi:10.24963/ijcai.2018/505

[24] Ailing Zeng, Muxi Chen, Lei Zhang, and Qiang Xu. 2023. Are transformers effective for time series forecasting?. In *Proceedings of the Thirty-Seventh AAAI Conference on Artificial Intelligence and Thirty-Fifth Conference on Innovative Applications of Artificial Intelligence and Thirteenth Symposium on Educational Advances in Artificial Intelligence (AAAI'23/IAAI'23/EEAI'23)*. AAAI Press, Article 1248, 8 pages. doi:10.1609/aaai.v37i9.26317

[25] Ling Zhao, Yujiao Song, Chao Zhang, Yu Liu, Pu Wang, Tao Lin, Min Deng, and Haifeng Li. 2019. T-GCN: A temporal graph convolutional network for traffic prediction. *IEEE transactions on intelligent transportation systems* 21, 9 (2019), 3848–3858.